energies

MDPI

Article

Medium-Temperature Heat Pumps for Sustainable Urban Heating: Evidence from a District Network in Italy

Mosè Rossi [1,*], Danilo Salvi [2] and Gabriele Comodi [1]

[1] Department of Industrial Engineering and Mathematical Sciences, Marche Polytechnic University, Via Brecce Bianche 12, 60131 Ancona, Italy; g.comodi@univpm.it
[2] Astea S.p.A., Via Guazzatore 163, 60027 Osimo, Italy; danilo.salvi@gruppoastea.it
* Correspondence: mose.rossi@staff.univpm.it; Tel.: +39-071-220-4430

Abstract

The decarbonisation of urban heating systems represents a key challenge for the transition towards sustainable cities. This study investigates the field integration of a Medium-Temperature Heat Pump (MTHP) within the Osimo District Heating Network (DHN) in Italy, demonstrating how low-grade return flows (30–50 °C) can be effectively upgraded to supply temperatures of 65–75 °C, in line with 4th-generation district heating requirements. Specifically, 5256 h of MTHP operation within the DHN were analysed to validate the initial design assumptions, develop surrogate performance models, and assess the system's techno-economic and environmental performance. The results indicate stable and reliable operation, with a weighted average Coefficient of Performance (COP) of 3.96 and a weighted average thermal output of 134.5 kW. From an economic perspective, the system achieves a payback period of approximately six years and a Levelised Cost of Heat (LCOH) of 0.0245 €/kWh. Environmentally, the MTHP enables CO_2 emission reductions of about 120 t compared with conventional gas-fired boilers. Beyond its technical performance, the study highlights the strong replicability of MTHP solutions for small- and medium-scale DHNs across Europe. The proposed approach offers urban utilities a scalable and cost-competitive pathway towards low-carbon heat supply, directly supporting municipal climate strategies and aligning with key EU policy frameworks, including the European Green Deal, REPowerEU, and the "Fit-for-55" package.

Keywords: climate-neutral heating; district heating decarbonisation; medium-temperature heat pump; sustainable cities; urban energy systems; waste heat recovery

Academic Editors: Mahmoud Bourouis and Xiaohu Yang

Received: 30 November 2025
Revised: 26 December 2025
Accepted: 19 January 2026
Published: 22 January 2026

1. Introduction

The urgent need to decarbonise energy production is central to mitigating climate change following decades of unsustainable human activity. In response, the European Union (EU) has introduced a set of ambitious policy frameworks to accelerate the energy transition, including the European Green Deal [1], the REPowerEU plan [2], and the revised Renewable Energy Directive (RED) III [3], which establish binding 2030 targets for renewable energy deployment and energy efficiency. These initiatives are further reinforced by the "Fit-for-55" package [4], which sets the pathway towards climate neutrality by 2050. Alongside the large-scale deployment of renewable energy technologies, such as solar [5], wind [6], hydropower [7], and biomass [8], Heat Pumps (HPs) powered by low-carbon electricity have emerged as a key solution for end-use electrification. HPs play an

increasingly important role in reducing greenhouse gas emissions across both residential and industrial sectors [9–11].

In residential applications, High-Temperature Heat Pumps (HTHPs) are generally defined as units capable of delivering supply temperatures above 65 °C, whereas in industrial contexts the high-temperature threshold typically exceeds 80–100 °C. Systems with maximum supply temperatures around 75 °C therefore fall below the industrial high-temperature definition but remain fully compatible with residential classifications. Such systems are more appropriately referred to as Medium-Temperature Heat Pumps (MTHPs), making them particularly suitable for small-scale 4th-generation DHNs (see Table 1).

Table 1. Common temperature classification of HPs.

Class Name	Typical Maximum Supply Temperature (°C)	Main Applications	Key Literature Review/Standards
Low-temperature	≤45–50	Underfloor heating, low-temperature DHN, pools	[12]
Medium-temperature	ca. 50–80	Domestic retrofit, small-scale 4th-generation DHN, low-temperature industry	[13]
High-temperature	≥80–100 (some definitions use ≥100)	Industrial process heat, high-return DHN, steam	[14,15]

Recent advances in MTHPs and HTHPs have significantly expanded their range of applications, particularly within the 50–100 °C supply temperature interval that characterises many medium-grade industrial process heat uses and 4th-generation DHNs. Ma et al. [16] reviewed compression-based MTHP and HTHP steam systems and demonstrated that, when recovering industrial waste heat in the 50–100 °C range, these technologies outperform electric, coal-fired, and gas-fired boilers for steam production, with associated CO_2 emission reductions strongly dependent on the electricity mix. Their analysis identified key Research and Development (R&D) priorities, including improvements in system efficiency; higher achievable steam temperatures; the development of high-temperature refrigerant, particularly R718 (water), owing to its zero Ozone Depletion Potential (ODP), zero Global Warming Potential (GWP), and high critical temperature; and advances in high-compression-ratio compressor technologies. Fernández-Moreno et al. [17] highlighted the growing importance of thermal energy storage in supporting MTHP and HTHPs operation. While underscoring the continued relevance of careful refrigerant selection and cycle configuration, they showed that robust thermal storage solutions can substantially reduce reliance on physical prototyping by enabling reliable and cost-effective dynamic performance modelling. However, they also identified a notable research gap: despite the wide availability of modelling approaches, integrated frameworks that effectively couple HP models with thermal storage and system-level simulation tools remain limited, a need directly addressed by the present study. Robbins et al. [18] investigated alternative control strategies for adsorption HPs operating with low-grade thermal sources in the 50–100 °C range. Their results demonstrated that adaptive control approaches, such as variable switching times and dynamic cycle optimisation, can enhance seasonal performance factors by up to 12% compared with conventional fixed-cycle control. These findings underline the strong potential of control optimisation in maintaining high efficiency under fluctuating source temperature conditions, which is particularly relevant for MTHP applications. Similarly, Li et al. [19] analysed the performance of a transcritical CO_2 HP for waste heat recovery in the 50–100 °C range supplying a 4th-generation DHN. By optimising gas cooler pressure and implementing partial-load control, the system achieved Coefficient of Performance (COP) improvements of 8–15% relative to baseline operation while delivering supply temperatures

of up to 90 °C. An economic assessment indicated payback periods between 3 and 5 years, depending on the stability of the heat source temperature and prevailing electricity prices. Finally, Yu et al. [20] experimentally evaluated HTHP performance across various internal heat exchanger, economiser, and subcooler configurations at supply temperatures between 85 and 125 °C. Results within the lower segment of this range (85–100 °C) are directly applicable to medium-grade applications, with the vapour-only injection mode achieving an 11.97% increase in heating capacity, a 4.43% improvement in COP, and a payback period of 1.44 years. Component-level insights into exergy losses and subcooling effects provide transferable guidance for optimising MTHP system design.

Beyond medium-grade industrial process heat applications, MTHPs are increasingly deployed in DHNs operating below 100 °C. In particular, they are well suited to 4th-generation DHNs, typically operating in the 70–95 °C range [21,22], as well as 5th-generation systems, characterised by ultra-low network temperatures of 15–45 °C [23,24]. This broad operating range makes MTHPs highly relevant for medium-temperature applications within urban energy systems. Mateu-Royo et al. [25] investigated the integration of MTHPs into DHNs under two distinct operating configurations: (i) return-side integration, in which the DHN acts as the heat consumer, and (ii) supply-side integration, in which the DHN acts as the heat supplier. In the return-side configuration, the MTHP achieved COP values between 3.2 and 5.4, resulting in operating cost reductions of at least 50%. Under supply-side operation, COP values ranged from 2.8 to 5.7, confirming the strong potential of MTHPs to improve efficiency and reduce costs in both supply-side and return-side DHN integration schemes. Vivian et al. [26] analysed the performance of booster HPs in 5th-generation DHNs, highlighting the rated network temperature difference defined at the design stage as a critical parameter for balancing capital investment and operating costs. From an economic standpoint, the proposed system was competitive with individual gas boilers, as it enables the recovery of heat from local low-temperature sources with minimal additional infrastructure requirements. Barco-Burgos et al. [27] provided a comprehensive review of MTHP integration into DHNs, identifying twelve generic connection configurations, four of which had not been previously reported in the literature. Their analysis showed that 3rd- and 4th-generation DHNs represent the most commonly studied reference cases. For centrally located HPs coupled with Combined Heat and Power (CHP) plants, typical COP values ranged between 3 and 4. In contrast, the use of local HPs in 4th- and 5th-generation DHNs resulted in lower COP values (0.95–1.5), while individual HPs connected within DHNs achieved higher COP values in the range of 3–4. This latter configuration is consistent with the findings of the present study, which are discussed in detail in the Section 5.

Despite these advances, only a limited number of studies have experimentally characterised MTHPs recovering low-grade waste heat at 30–50 °C to deliver supply temperatures of up to 75 °C, a configuration particularly relevant for small-scale 4th-generation DHNs. Addressing this gap, this study provides the following contributions:

- Extended field operation case study: Analysis of 5256 h of on-site operation of a vapour-compression MTHP recovering low-grade waste heat at 30–50 °C and supplying heat at up to 75 °C to a small 4th-generation DHN. Over the reference year (8760 h), the system operated for 60% of the total annual hours, and this operating duration formed the basis of the performance assessment. The MTHP achieved a weighted average COP of 3.96 and a thermal output of 134.5 kW, both within 1% of the design values.
- Reproducible, multi-path workflow: Realisation of an open Python (version 3.9) framework with three complementary paths: (A) validation and normalisation of COP, Carnot COP, second-law efficiency (η_{II}), and uncertainty propagation; (B) surrogate modelling of η_{II} as a function of thermodynamic lift (ΔT_{lift}), defined as the difference

between the DHN supply temperature at the HP outlet and the DHN return temperature at the HP inlet ($T_{DHN,supply} - T_{DHN,return}$), and mass flow of the DHN return line ($\dot{m}_{DHN,\ return}$); and (C) techno-economic and environmental assessment.

- From COP to η_{II}: Benchmarking COP against Carnot COP and η_{II} to assess proximity to thermodynamic limits.
- Design-to-field fidelity: Direct comparison between measured and design condenser powers to verify performance reliability.
- Clear DHN context: Positioning the unit within the medium-temperature supply band of small DHNs, bridging residential and industrial classifications, and aligning with 4th- and 5th-generation DHN practices.

2. Overview of the MTHP Technology

A MTHP is a closed-loop thermodynamic system designed to upgrade low-grade waste heat from a cold source to a medium-temperature heat supply, typically within the 70–95 °C range, by means of external mechanical work. In the configuration investigated in this study, the MTHP comprises the following main components: (a) evaporator (EV), which extracts thermal energy from the cold source, here operating in the 30–50 °C range, causing the working fluid to evaporate from the liquid to the vapour phase and enabling heat transfer into the cycle; (b) two modulating compressors (C1 and C2), which compress the refrigerant vapour from the evaporator pressure to the condenser pressure. The compressors adjust the refrigerant mass flow rate in response to the available source heat, thereby optimising performance under variable load and temperature lift conditions; (c) condenser (CO), which delivers the upgraded thermal energy to the heat sink by condensing the working fluid from vapour to liquid or a two-phase mixture, supplying temperatures of up to 75 °C suitable for small 4th-generation DHN operation; (d) expansion (lamination) valve (LV), which reduces the refrigerant pressure, ideally under isenthalpic condition, before the fluid re-enters the evaporator, thus closing the thermodynamic cycle. In some configurations, an additional recuperator (RE) is incorporated to enhance system efficiency by transferring heat from the high-pressure liquid line to the low-pressure vapour in the compressor suction line. This internal heat exchange reduces superheating requirements and increases liquid subcooling, leading to improved overall performance. Figure 1 illustrates the layout of the MTHP analysed in this work.

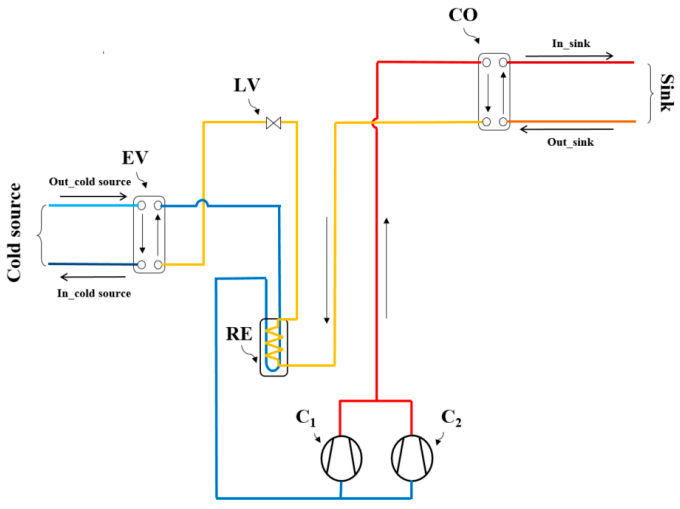

Figure 1. Layout of the analysed MTHP, including the evaporator (EV), two modulating compressors (C1, C2), condenser (CO), expansion valve (LV), and recuperator (RE). Colour coding represents the refrigerant temperature levels along the cycle, with red, yellow, and blue indicating high, intermediate, and low temperatures, respectively.

3. Case Study

The MTHP application analysed in this study is implemented within the small-scale, 4th-generation DHN of Osimo, located in the Marche region of Italy [28,29]. The system is primarily supplied by natural-gas-fired boilers, two units rated at 4.6 MW_{th} and one unit rated at 4.2 MW_{th}, with one boiler operated as a backup, together with a CHP plant rated at 1.2 MW_{el} and 1.3 MW_{th}. These units collectively supply the only DHN currently in operation in the region. The network supplies approximately 3% of the town's total heat demand and is located in climatic zone D (−2 °C to 34 °C), serving both residential and small tertiary users. The DHN operates with supply temperatures in the range of 65–75 °C, while return temperatures typically lie between 30 °C and 50 °C. From an energy and environmental perspective, the Osimo case demonstrates that DHNs based on natural gas-fired boilers and CHP units can already achieve significant primary energy savings and CO_2 emission reductions compared with boiler-only configurations. At the same time, the presence of stable return water streams in the 30–50 °C temperature range provides particularly favourable boundary conditions for the integration of MTHPs. Although the Osimo DHN supplies only a limited share of the local heat demand, it represents a valuable urban-scale demonstrator of how medium-sized municipalities can integrate innovative low-carbon technologies into existing heating infrastructures, thereby paving the way for replication in similar European towns.

Within this context, Corradi et al. [28] established a comprehensive baseline characterisation of the CHP-based DHN, analysing its energy, environmental, and economic performance without considering HP integration. Building on that reference framework, Mugnini et al. [29] explored system-level retrofit strategies through dynamic simulations, assessing the effects of temperature reduction and HP deployment as a booster for peak loads, with a focus on network-wide indicators. In contrast, this study addresses a complementary and more technology-oriented research question, providing the experimental field validation and thermodynamic characterisation of an MTHP integrated into the same DHN. Based on 5256 h of measured operation, it focuses on continuous base-load operation, direct design-to-field performance validation, and detailed efficiency metrics (COP, Carnot COP, and second-law efficiency). In addition, surrogate models and a component-level techno-economic assessment are introduced to support the replicability of this near-term retrofit solution in small- and medium-scale DHNs. For clarity, Figure 2 illustrates the schematic integration of the MTHP within the Osimo DHN, highlighting the coupling between the DHN return line, the HP, and the supply line.

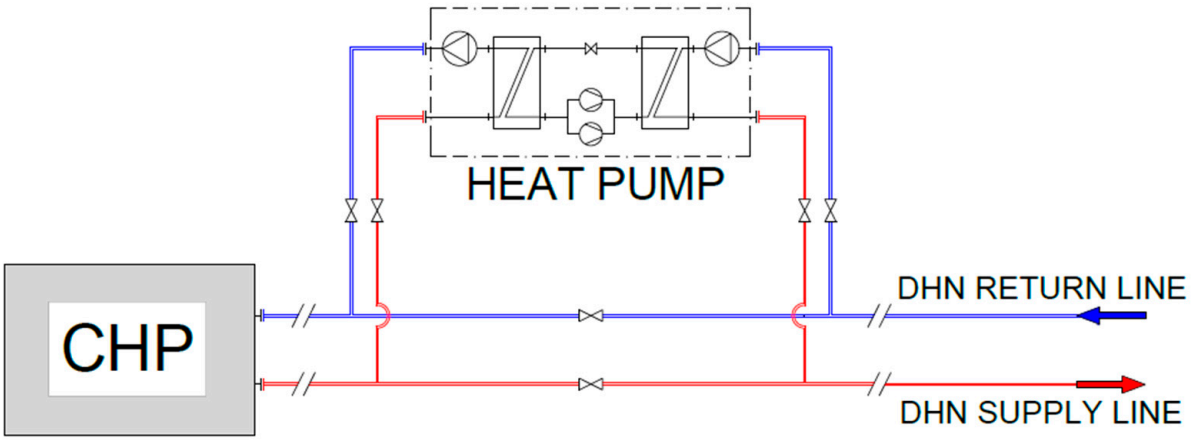

Figure 2. Schematic of the MTHP integration within the DHN, showing the coupling between the return line, the HP, and the supply line.

4. Design and Methodological Framework of the MTHP

This section outlines the methodological framework adopted to evaluate performance, validate the design assumptions, and assess the techno-economic potential of the investigated MTHP for low-grade waste heat recovery in a 4th-generation DHN. The methodology is structured into five main steps:

- DHN return line characterisation (Section 4.1).
- DHN supply line characterisation and design-phase output estimation (Section 4.2).
- System configuration and refrigerant selection (Section 4.3).
- Measurement and data acquisition (Section 4.4).
- Multi-path analysis workflow (Section 4.5), including
    - Path A: Performance validation and Carnot benchmarking.
    - Path B: Surrogate modelling for performance mapping and operating-condition analysis.
    - Path C: Techno-economic and environmental assessment.

To provide a clear overview, the methodological workflow adopted in this study is illustrated in Figure 3. The workflow summarises the entire analysis process, from the definition of system boundaries and design-stage calculations to system configuration and data acquisition, and finally to the multi-path analysis comprising performance validation (Path A), surrogate modelling (Path B), and techno-economic and environmental assessment (Path C).

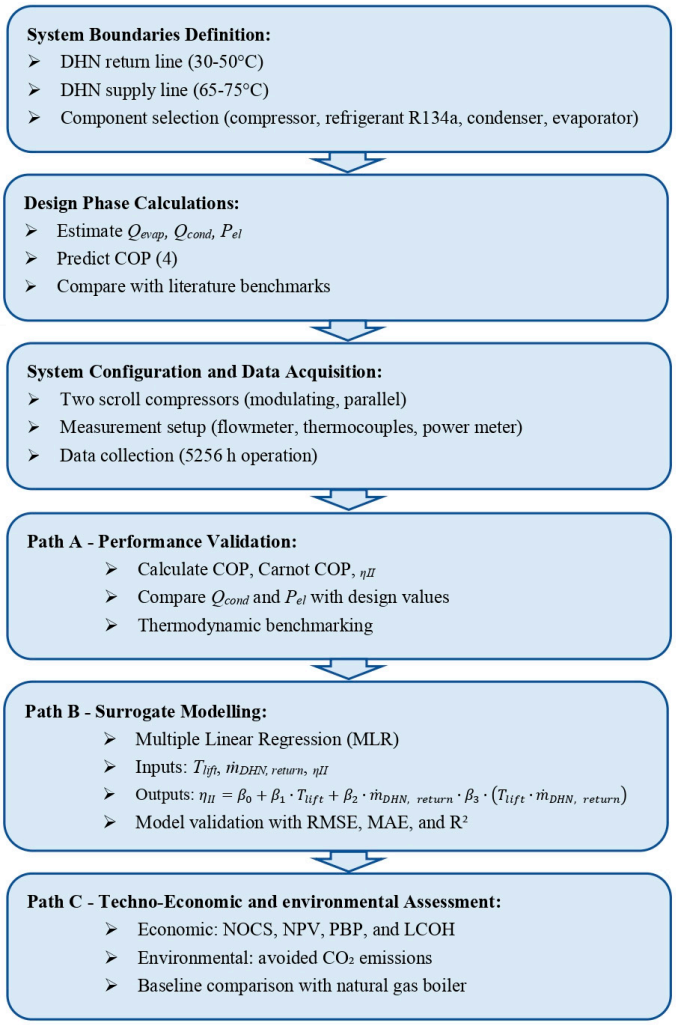

Figure 3. Methodological workflow adopted for the design, validation, and techno-economic and environmental assessment of the investigated MTHP.

4.1. DHN Return Line Characterisation

In this study, the cold source is represented by the DHN return line, operating in the temperature range of 30–50 °C. The working fluid in the DHN return line-EV circuit for the investigated MTHP is a 35% vol. ethylene glycol–water mixture, selected for its low freezing point and stable thermal properties in the operating temperature range. Both the fluid density (ρ) and the specific heat capacity at constant pressure (c_p) are temperature dependent, and their accurate evaluation is essential for correctly estimating the available thermal power and, consequently, for the proper sizing of the EV. Within the temperature range relevant to this application (36.0–46.3 °C), the density decreases slightly from 1045 kg/m^3 to 1040 kg/m^3, while c_p increases marginally from 3.608 kJ/kg·°C to 3.639 kJ/kg·°C. Although these variations are modest, they are explicitly accounted for in the calculations to minimise systematic errors in the performance assessment. Using the weighted average inlet and outlet temperatures of the working fluid over the monitored period (43.1 °C and 38.9 °C, respectively), the corresponding mean thermophysical properties are ρ_{in_EV} = 1044.28 kg/m^3, ρ_{out_EV} = 1042.31 kg/m^3, c_{pin_EV} = 3.617 kJ/kg·°C, and c_{pout_EV} = 3.630 kJ/kg·°C. The measured mass flow rate of the working fluid ($\dot{m}_{EV}$) varied between 5.9 kg/s to 6.8 kg/s with a weighted average value of 6.7 kg/s. Combined with the observed temperature difference across the EV (ΔT_{EV} = 3.4–4.4 °C, weighted average = 4.2 °C), the thermal power absorbed at the EV is calculated through Equation (1):

$$Q_{evap}\ [kW] = \dot{m}_{EV}\left[\frac{kg}{s}\right]\cdot c_p\left[\frac{kJ}{kg\ \times\ ^\circ C}\right]\cdot \Delta T_{EV}\ [^\circ C] \quad (1)$$

Using the weighted average operating conditions, the EV absorbed a mean thermal power of 101.4 kW, with instantaneous values ranging from 73.1 kW to 108.7 kW. The relatively narrow range of thermal power observed reflects the high stability of the DHN return line operating conditions, which is advantageous for both COP consistency and the robustness of surrogate model fitting. In addition, the modest temperature lift between the DHN return line and the DHN supply line (see Section 4.2) makes this application particularly well-suited to MTHP operation, as it enables high seasonal efficiency without imposing excessive loads on the compressors. In the literature, MTHPs integrated into DHNs often experience significantly higher DHN return line variability, with seasonal temperature swings of up to 10–15 °C and mass-flow fluctuations exceeding 20% [25,26]. By contrast, the DHN return line analysed in this study exhibits exceptional operational stability, with temperature deviations confined to within ±2 °C of the mean and mass-flow variations limited to less than 15% over the entire monitoring period. Such tightly bounded operating conditions, rarely reported in comparable DHN-integrated MTHP applications, substantially reduce transient-induced performance fluctuations. As also shown in [29], these limited variations have a negligible impact on overall system efficiency. Table 2 lists the main operating magnitudes related to the EV, in terms of both the range and the weighted average values, used for MTHP design and derived from the operational dataset. Specifically, each weighted average value reflects the frequency of occurrence of the corresponding variable within the observed range over the monitoring period.

Table 2. Operating ranges and weighted average values used for the MTHP design.

Magnitude [Unit of Measure]	Range	Weighted Average Value
T_{out_EV} [°C]	39.4–46.3	43.1
T_{in_EV} [°C]	36.0–41.9	38.9
ΔT_{EV} [°C]	3.4–4.4	4.2
$\dot{m}_{EV}$ [kg/s]	5.9–6.8	6.7
Q_{evap} [kW]	73.1–108.7	101.4

4.2. DHN Supply Line and Design-Phase Output Estimation

On the DHN supply line, the fluid operates in a higher temperature range of 65–75 °C, which aligns with the supply temperature requirements for small 4th-generation DHN under investigation. Also in this case, the working fluid in the DHN supply line-CO circuit for the investigated MTHP is 35% vol. ethylene glycol–water mixture, ensuring compatibility and simplifying maintenance requirements. From the EV performance determined in Section 4.1 (Q_{evap} ranging from 73.1 kW to 108.7 kW, weighted average 101.4 kW), the CO output is estimated by accounting for the electrical input to the two modulating scroll compressors. Based on manufacturer specifications and preliminary monitoring, the combined electrical power consumption (P_{el}) ranges from 24.4 kW to 36.2 kW, with a weighted average of 33.8 kW under nominal load. The design-phase calculations assume a nominal COP of 4, consistent with values reported in the literature for comparable MTHP systems [25,27]. The COP is defined as in Equation (2):

$$COP\ [-] = \frac{Q_{evap}\ [kW] + P_{el}\ [kW]}{P_{el}\ [kW]} = \frac{Q_{cond}\ [kW]}{P_{el}\ [kW]} \quad (2)$$

Using the bounds of both Q_{evap} and P_{el}, the design-phase Q_{cond} values are as follows: minimum 97.5 kW (low EV load + low compressor input), maximum: 144.9 kW (high EV load + high compressor input), and weighted average: 135.2 kW (nominal operating point). These output values correspond to a temperature lift between the DHN return and supply lines of 27–36 °C, which lies within the optimal operating range for compressors. This moderate temperature lift is a key contributor to the high predicted COP, as larger temperature lifts (>40 °C) are known to increase compressor discharge temperatures and significantly reduce cycle efficiency [30]. From an application perspective, the DHN supply line operating range of 65–75 °C provides sufficient supply temperatures for space heating in 4th-generation DHNs, as in the case study examined here, while maintaining a favourable balance between efficiency, thermal coverage, and compressor durability. This avoids the operational penalties typically associated with HTHPs operating above 90 °C [31]. To contextualise these design-phase estimates, Table 3 compares the CO thermal output and COP values obtained in this study with literature data for MTHPs operating in the 50–100 °C supply temperature range. As shown, the Q_{cond} range of 97.5–144.9 kW (weighted average 135.2 kW) aligns well with the mid-to-upper range of values reported for similar systems in DHNs and industrial waste heat recovery applications. The nominal COP of 4 obtained at the calculated temperature lift of 27–36 °C is competitive with, and in several cases exceeds, the performance reported in the literature for systems operating under comparable conditions.

4.3. System Configuration and Refrigerant Selection

The MTHP is equipped with two scroll-type, modulating compressors rated at 20 kW each and arranged in parallel. This configuration provides both load flexibility and operational redundancy, ensuring continuity of service in the event of maintenance or component failure. The parallel arrangement also enables staged operation, allowing the system to maintain higher efficiency under part-load conditions during periods of reduced heat demand. Scroll compressors are particularly well suited to the moderate temperature lift of this application (27–36 °C), as they offer high isentropic efficiency at low-to-medium pressure ratios, exhibit minimal internal leakage, and require simpler lubrication management compared with reciprocating or screw compressors. In addition, the relatively low discharge temperatures expected under these operating conditions contribute to enhanced compressor reliability and long service life.

Table 3. Comparison of Q_{cond} for MTHPs operating at 50–100 °C.

Study	Application/Heat Source	DHN Supply Line Temperature Range [°C]	Q_{cond} [kW]	COP	Notes
This work	DHN integration (glycol–water, 35% vol.)	65–75	97.5–144.9 (weighted average 135.2)	4.0	Two scroll compressors, R134a, stable DHN return line
[17]	Industrial waste heat recovery	50–100	80–170	3.0–4.5	Emphasis on R&D gaps and modelling approaches
[19]	CO_2 transcritical HP (waste heat recovery)	70–90	100–140	3.5–4.0	Optimised gas cooler pressure, partial load control
[25]	DHN (water)	60–75	80–150	3.2–5.7	Performance varies with mode: DHN as sink or source
[26]	Booster HP in 5th-generation DHN	55–75	60–110	3.0–4.8	Emphasis on design ΔT and economic trade-offs
[27]	DHN integration (waste heat)	60–90	90–160	2.8–4.5	4th-gen network with local HPs

The selected working fluid, R134a, is well suited to the EV and CO temperature ranges identified in Sections 4.1 and 4.2. Its favourable thermophysical properties, moderate operating pressures, relatively high critical temperature, and proven compatibility with scroll compressor technology enable stable operation in the 65–75 °C DHN supply line temperature range without approaching critical limits. At the rated design point (flash-off = 25 °C, dew point = 75 °C), the system achieves a Q_{cond} of 135.2 kW, P_{el} of 33.8 kW, COP of 4, and $\dot{m}_{R134a}$ of 0.475 kg/s. The design includes 3 °C of subcooling at the CO outlet to increase refrigerant density and improve volumetric efficiency, and 5 °C of superheating at the compressor suction to ensure complete vaporisation of the refrigerant prior to compression, thereby preventing liquid slugging and protecting compressor integrity.

4.4. Measurement and Data Acquisition

The CO heat output (Q_{cond}) was measured using a combination of flow and temperature instrumentation to allow direct calculation via the energy balance Equation (3):

$$Q_{cond}\,[kW] = \dot{m}_{CO}\left[\frac{kg}{s}\right]\cdot c_p\left[\frac{kJ}{kg\ \times\ ^\circ C}\right]\cdot \Delta T_{CO}\,[^\circ C] \quad (3)$$

Specifically:

- An ultrasonic flowmeter (IP67 protection class) was installed on the DHN supply line-side liquid line to measure the volumetric flow rate of the glycol–water mixture. Ultrasonic technology was selected for its non-intrusive operating principle, wide turndown ratio (0.6–100 m^3/h), and suitability for fluids with variable thermophysical properties.
- Two type-K thermocouples (IP67 protection class) were installed immediately upstream and downstream of the CO to measure the temperature difference across the heat exchanger (ΔT_{CO}) with high temporal resolution. The sensor accuracy (±1.5% over the −50 to 1000 °C range) ensures reliable detection of the relatively small temperature lifts characteristic of this application.

The combined measurements from the flowmeter and thermocouples allow direct calculation of the CO thermal output Q_{cond} and comparison with the design-phase values

(Section 4.2). The electrical input power to the compressors (P_{el}) was measured using a semi-direct energy meter, with voltage measured directly and current sensed via a calibrated current transformer. Data acquisition is handled through a Metre-Bus (M-Bus) interface and automatically logged to a local Structured Query Language (SQL)-based database, enabling high-frequency, unattended monitoring and subsequent post-processing for load and performance analysis. Figure 4 shows the installed instrumentation, with the ultrasonic flowmeter highlighted in blue and the thermocouples in red, while Table 4 summarises the main technical specifications of the measurement devices.

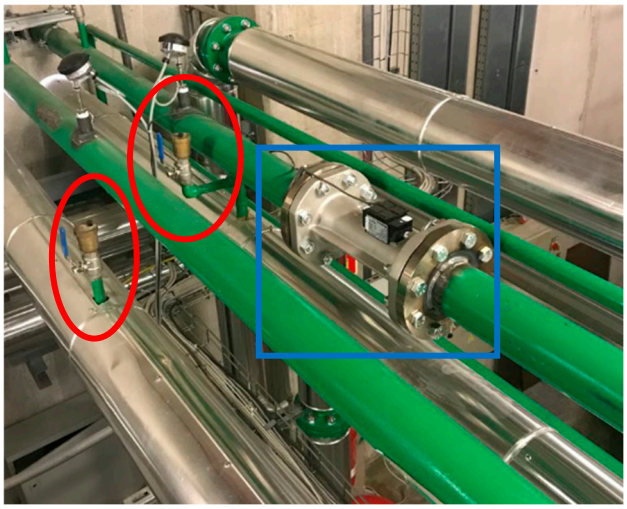

Figure 4. Equipment for Q_{cond} measurement (flowmeter in blue, thermocouples in red).

Table 4. Technical specifications of measurement equipment.

Equipment	Protection Class	Measurement Range	Accuracy (%)	Output Signal
Ultrasonic flow metre	IP67	0.6–100 m^3/h	±3.5	4.096 mV
Thermocouple (Type K)	IP67	−50–1000 °C	±1.5	4.096 mV

4.5. Multi-Path Analysis Workflow

The MTHP performance dataset was analysed through three complementary and interconnected pathways. This modular framework enables the robust validation of design assumptions, parametric modelling of system behaviour, and a quantitative assessment of the associated exergy and economic implications.

4.5.1. Path A—Performance Validation

This path focuses on the thermodynamic validation of the system against the design specifications. Using the measured Q_{cond} and P_{el}, the COP is calculated. For benchmarking, the corresponding Carnot COP, based on measured cold source and sink temperatures, is also computed along with η_{II}, defined as the ratio of actual to ideal performance, according to Equations (4) and (5), respectively.

$$COP_{Carnot}\ [-] = \frac{T_{sink}\ [K]}{T_{sink}\ [K] - T_{cold}\ [K]} \tag{4}$$

$$\eta_{II}[-] = \frac{COP\ [-]}{COP_{Carnot}\ [-]} \tag{5}$$

The validated dataset is then used to generate the core performance plots: COP versus temperature lift, η_{II} versus the temperature lift, and Q_{cond} versus temperature lift. These

plots serve as the baseline for assessing whether the field operating points align with expected thermodynamic behaviour and literature benchmarks for MTHPs.

4.5.2. Path B—Surrogate Modelling

This path develops a surrogate model to describe the relationship between MTHP performance and its key operating parameters. A bilinear Multiple Linear Regression (MLR) formulation is adopted to account for interaction effects and provide an interpretable analytical representation of system behaviour. Monthly surrogate models are calibrated alongside an overall model for the dataset. Model predictions are visualised using three-dimensional response surfaces, and model accuracy is evaluated using the Root Mean Square Error (RMSE), Mean Absolute Error (MAE), and coefficient of determination (R^2).

4.5.3. Path C—Techno-Economic and Environmental Assessment

The third path assesses the economic and environmental performance of the MTHP by combining measured operational data with relevant market and policy parameters. The analysis quantifies potential cost savings and CO_2 emission reductions, thereby evaluating the system's competitiveness relative to conventional heating technologies. The economic assessment estimates avoided fuel costs by comparing MTHP operation with a reference natural gas boiler of equivalent thermal output, while the environmental assessment quantifies the associated CO_2 savings resulting from the displacement of fossil-fuel heating. Results are expressed in terms of

- Net Operating Cost Savings (NOCS) (€), Equations (6)–(8).
- Net Present Value (NPV) (€), PBP (yr), and Levelised Cost of Heat (LCOH), Equations (9)–(11).
- Avoided CO_2 emissions ($kgCO_2/yr$), Equations (12)–(14).

In particular:

$$C_{NG}[€] = \sum_1^{OHs} \frac{Q_{cond,\,i}[kW]\cdot h_i\ [h]}{\eta_{th}\ [-]} \cdot c_{NG}\left[\frac{€}{kWh}\right] \tag{6}$$

$$C_{HP}[€] = \sum_1^{OHs} \frac{Q_{cond,\,i}[kW]\cdot h_i\ [h]}{COP_i\ [-]} \cdot c_{el}\left[\frac{€}{kWh}\right] \tag{7}$$

$$NOCS\ [€] = C_{NG}[€] - C_{HP}[€] \tag{8}$$

$$NPV\ [€] = -CAPEX\ [€] + \sum_{t=1}^{n} \frac{NOCS_t\ [€] - OPEX_t\ [€]}{(1+r)^t} \tag{9}$$

$$PBP\ [yr] = min\left[t : \sum_{i=1}^{t} (NOCS_i[€] - OPEX_i\ [€]) \geq CAPEX\ [€]\right] \tag{10}$$

$$LCOH\left[\frac{€}{kWh}\right] = \frac{\sum_{t=1}^{n} \frac{CAPEX_t[€]}{(1+r)^t} + \sum_{t=1}^{n} \frac{OPEX_t[€]}{(1+r)^t}}{\sum_{t=1}^{n} (Q_{cond}\cdot OHs)_t\ [kWh]} \tag{11}$$

$$CO_2{}^{NG}[kgCO_2] = \sum_1^{OHs} \frac{Q_{cond,\,i}[kW]\cdot h_i}{\eta_{th}\ [-]} \cdot EF_{NG}\left[\frac{kgCO_2}{kWh}\right] \tag{12}$$

$$CO_2{}^{HP}[kgCO_2] = \sum_1^{OHs} \frac{Q_{cond,\,i}[kW]\cdot h_i}{COP_i\ [-]} \cdot EF_{el}\left[\frac{kgCO_2}{kWh}\right] \tag{13}$$

$$\Delta CO_2[kgCO_2] = CO_2{}^{NG}[kgCO_2] - CO_2{}^{HP}[kgCO_2] \tag{14}$$

5. Results and Comments

This section presents the field validation of the MTHP under real operating conditions, its comparison with design-phase predictions, and the subsequent analysis of performance

distributions. The unit was deployed for low-grade waste heat recovery from a stable DHN return line and operated in heating mode to supply a glycol–water loop at temperatures of 65–75 °C. The measurement campaign covered the year 2021 and yielded a total of 5256 h of recorded operation.

5.1. Time Series Performance Overview (Path A)

Figure 5 shows the time series of measured COP and Q_{cond}. The MTHP operated for a total of 5256 h, predominantly near its nominal design point, with a weighted average COP of 3.96 vs. design assumption of 4; with a relative deviation of 1.01%; a weighted average Q_{cond} of 134.53 kW vs. design value of 135.2 kW; a relative deviation of 0.53%; a maximum Q_{cond} of 142.50 kW vs. design value of 144.95 kW; a relative deviation of 1.72%; a minimum Q_{cond} of 96.17 kW vs. design value of 97.47 kW; a relative deviation of 1.35%; and a total thermal energy delivered of 705.5 MWh that, when referenced to the design-point output over the same operating hours, corresponds to 99.4% of the theoretical yield.

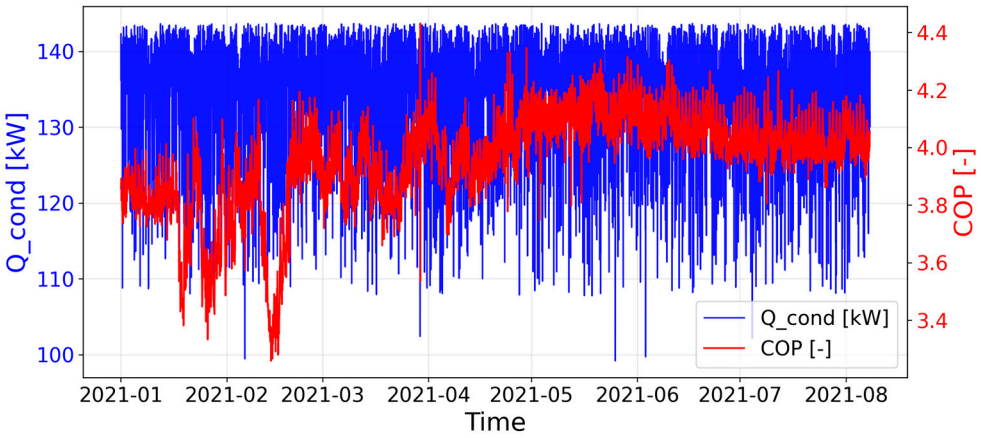

Figure 5. Time series of COP (right y-axis) and Q_{cond} (left y-axis).

Performance stability was further reinforced by the operating conditions of the DHN return line, which exhibited temperature variations within ±2 °C of the mean and mass-flow fluctuations below 15%. This limited variability constrains the temperature lift to a narrow range, thereby preventing significant COP degradation and minimising efficiency penalties associated with part-load operation. In this case, since the measured seasonal weighted average COP matched the design-point COP within 1%, negligible performance losses are obtained due to transient operation, thus reinforcing the suitability of the dataset for surrogate modelling (Path B) and benchmarking.

5.2. Performance Distribution and Analysis (Path A)

To further characterise the operational behaviour of the MTHP, the measured COP and Q_{cond} were analysed using frequency distributions (Figures 6 and 7). This approach provides insight into how often the system operates under optimal, suboptimal, and part-load conditions, offering an indirect assessment of both the adequacy of system sizing and the variability of the thermal demand on the DHN supply line.

Over the monitoring period, 94.8% of the recorded operating hours fall within a COP range of 3.5–4.5, indicating that the system operates predominantly under high-efficiency conditions. The most frequent COP class is 3.9–4.0, accounting for 15.3% of the total operating hours, which corresponds to near-nominal operation and closely matches the measured weighted average COP of 3.96. Operating hours with COP values above 4 (46.1%) are primarily associated with slightly reduced temperature lifts, typically resulting from lower DHN supply line set-points or marginally higher DHN return line temperatures.

Conversely, operation at COP values below 3, representing only 5.2% of the total hours, is infrequent and generally linked to periods of increased temperature lift, such as transient load peaks or atypical source conditions. The P10–P90 interval (3.76–4.14) encompasses 80% of all recorded COP values, providing a robust measure of the central dispersion of system performance while excluding extreme low- and high-efficiency outliers.

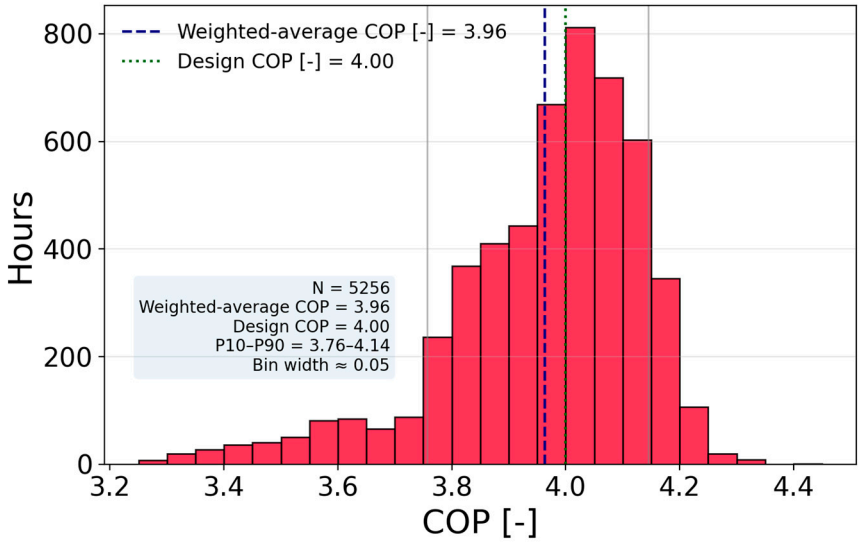

Figure 6. Histogram of COP with weighted average COP, design COP, and P10–P90 range.

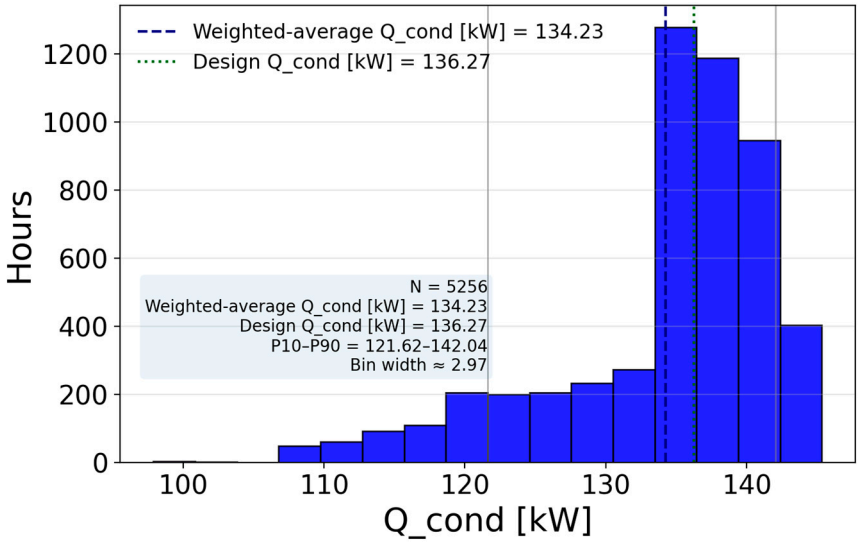

Figure 7. Histogram of Q_{cond} with weighted average COP, design COP, and P10–P90 range.

The distribution of thermal output is highly concentrated, with 76.4% of the operating hours falling within the 130–140 kW range, confirming that the system is well matched to its nominal design load and experiences minimal oversizing penalties. The most frequent output class is 138–141 kW, corresponding to operation within ±2.0% of the rated capacity (136.27 kW). The measured mean thermal output is 134.23 kW, while the P10–P90 interval (121.62–142.04 kW) indicates that 80% of the recorded values lie close to the design point. Operation at lower thermal loads (<125 kW) accounts for only 12.1% of the total operating hours and is primarily driven by variations in the thermal demand rather than by limitations of the DHN return line, consistent with the latter stable temperature and flow conditions discussed in Section 5.1. To complement the frequency distributions of COP and thermal

output (Figures 6 and 7), Figures 8–10 present monthly heat maps of COP, η_{II}, and Q_{cond} as functions of temperature lift and DHN return line mass flow rate.

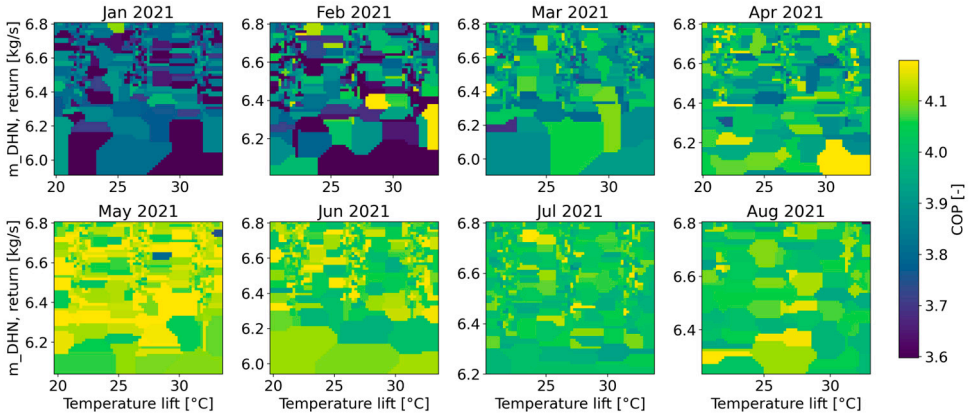

Figure 8. Monthly COP maps vs. temperature lift and DHN return line mass flow rate. Higher COP (>4) occurs at reduced lift (20–24 °C). Efficiency drops below 3.7 at temperature lifts >30 °C. Winter shows wider variability than summer.

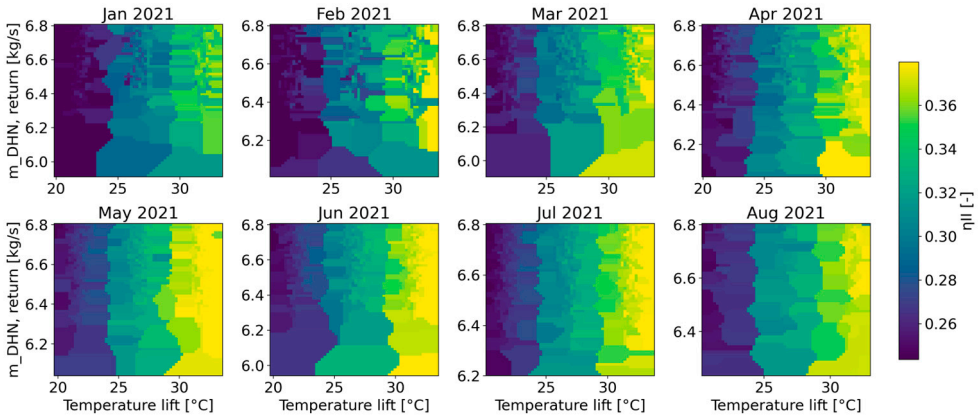

Figure 9. Monthly η_{II} maps vs. temperature lift and DHN return line mass flow rate. Best performance (ca. 0.37) at temperature lifts <24 °C. Efficiency falls below 0.28 above 30 °C. Temperature lift dominates behaviour, with stable summer operation.

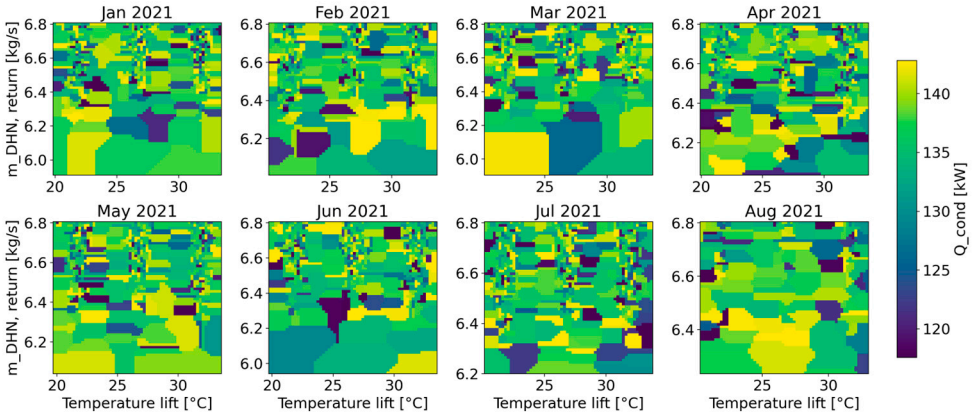

Figure 10. Monthly Q_{cond} maps vs. temperature lift and DHN return line mass flow rate. Output remains concentrated around 130–140 kW, matching design. Slight drops (<125 kW) in winter at high temperature lift; peaks (>140 kW) in summer at favourable conditions.

The COP distribution shows a clear dependence on the temperature lift, with values exceeding 4 predominantly associated with reduced temperature lift conditions (20–24 °C) and moderate DHN return line mass flow rates (approximately 6.3–6.6 kg/s). Conversely,

COP falls below 3.7 under high temperature lift conditions (>30 °C), particularly at the lower end of DHN return line mass flow rate. Seasonal effects are also evident. During the winter months (January–March), a wider dispersion of COP values is observed, reflecting the combined influence of higher thermal demand and lower DHN return line temperatures. In contrast, the summer period (May–August) is characterised by more uniform performance, with COP stabilising in the range of 3.9–4.1 even under moderate temperature lift conditions. Overall, these results confirm that the unit is appropriately sized to operate most of the time close to its design point, with noticeable performance degradation occurring only during peak winter load conditions.

The η_{II} maps confirm the trends observed for the COP, while more clearly highlighting performance degradation under higher temperature lift conditions. Peak efficiency values (approximately 0.37 in relative terms) are achieved when the lift remains below 24 °C, whereas operation at temperature lifts exceeding 30 °C consistently results in values below 0.28. These results indicate that system performance is primarily governed by the temperature lift, with DHN return line-side variations playing a secondary role. The relatively stable performance observed during the summer months further demonstrates the suitability of the unit for base-load operation under moderate temperature lift conditions. Conversely, the reduced efficiency observed in winter reflects the unavoidable thermodynamic penalty associated with higher DHN supply line temperature requirements.

Q_{cond} remains strongly concentrated in the 130–140 kW range across the entire operating envelope, confirming close alignment with the design capacity. Moderate reductions in output (<125 kW) occur primarily during the winter months (January–March) under conditions of high temperature lift and reduced DHN return line mass flow rate, coinciding with the lowest observed COP and second-law efficiency values. Conversely, peak thermal outputs exceeding 140 kW are occasionally achieved during the spring and early summer months (April–June), when both the temperature lift and DHN return line mass flow rate conditions are more favourable. Overall, the system consistently delivers near-nominal capacity across seasons, with deviations in performance largely attributable to temperature lift-induced efficiency effects rather than limitations on the DHN supply side.

5.3. Surrogate Model Observations (Path B)

The bilinear surrogate model, commonly applied in energy systems analyses [32], was calibrated to approximate the efficiency η_{II} as a function of temperature lift (T_{lift}) and $\dot{m}_{DHN,\,return}$. The general formulation is reported in Equation (15), while Table 5 shows the surrogate model coefficients of the monthly surrogates and the overall dataset:

$$\eta_{II} = \beta_0 + \beta_1 \cdot T_{lift} + \beta_2 \cdot \dot{m}_{DHN,\,return} \cdot \beta_3 \cdot \left(T_{lift} \cdot \dot{m}_{DHN,\,return} \right) \quad (15)$$

Table 5. Overall and monthly surrogate model coefficients.

Month	β_0	β_1	β_2	β_3
Overall	−0.0487	0.01281	0.01070	−0.000317
Jan 2021	0.0556	0.00787	−0.00485	0.000333
Feb 2021	0.0613	0.00701	−0.00621	0.000496
Mar 2021	0.0555	0.00945	−0.00427	0.000144
Apr 2021	0.0876	0.00774	−0.00969	0.000454
May 2021	0.0789	0.00815	−0.00855	0.000389
Jun 2021	0.0137	0.01164	0.00078	−0.000141
Jul 2021	−0.0276	0.01349	0.00637	−0.000340
Aug 2021	0.0906	0.00737	−0.01013	0.000468

Note: coefficients are dimensionless.

The estimation errors and reliability coefficients of the monthly surrogate model equations are summarised in Table 6. Overall, the models exhibit consistently low errors, with RMSE values ranging from 0.0079 to 0.0169, MAE values between 0.0063 and 0.0137, and coefficients of determination (R^2) spanning 0.87 to 0.97. When applied to the aggregated dataset, the surrogate model achieves an RMSE of 0.0136, an MAE of 0.0103, and an R^2 of 0.914, confirming its robustness across seasonal operating conditions.

Table 6. Errors and reliability coefficients of the monthly surrogate model equations.

Month	RMSE	MAE	R^2
Overall	0.0136	0.0103	0.914
Jan 2021	0.0113	0.0091	0.931
Feb 2021	0.0169	0.0137	0.870
Mar 2021	0.0080	0.0066	0.965
Apr 2021	0.0079	0.0063	0.969
May 2021	0.0081	0.0066	0.966
Jun 2021	0.0120	0.0093	0.934
Jul 2021	0.0115	0.0090	0.938
Aug 2021	0.0106	0.0081	0.949

From a technical standpoint, the highest predictive accuracy is observed during the spring months (March–April), when the reduced dispersion of operating conditions leads to improved model performance ($R^2 > 0.96$). In contrast, the lowest accuracy occurs in February, likely due to increased variability in operating points and a wider distribution of cold-source mass flow rates, which slightly degrades the model fit ($R^2 = 0.87$). Figure 11 illustrates the monthly three-dimensional scatter plots together with the fitted surrogate surfaces.

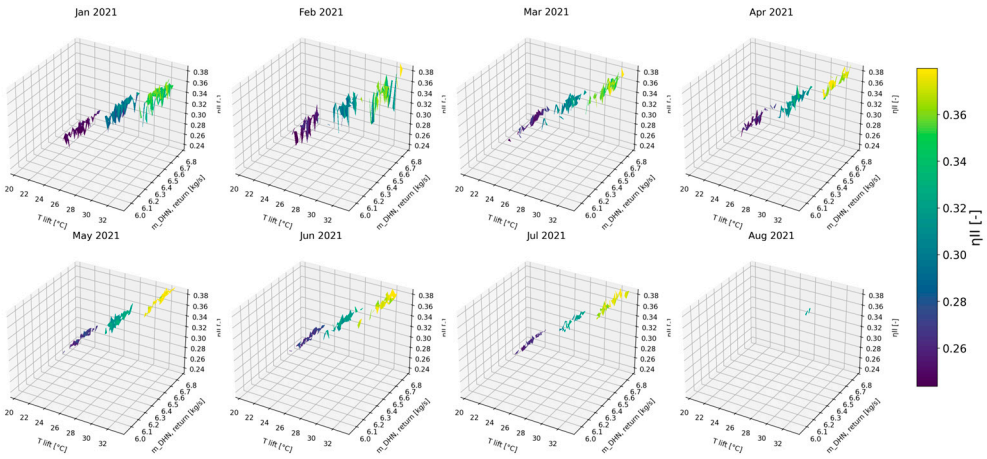

Figure 11. Monthly 3-D scatter plots of surrogate efficiency (η_{II}) vs. temperature lift (T_{lift}) and DHN return line mass flow rate ($\dot{m}_{DHN,\,return}$) (Jan–Aug 2021).

Efficiency exhibits a consistent inverse relationship with temperature lift, while the influence of the DHN return line mass flow rate is less pronounced overall but becomes more evident during the summer months, when a broader operating envelope accentuates interaction effects. Seasonal efficiency values range from approximately 0.24 to 0.38, with more tightly clustered distributions in winter and increased variability during summer.

5.4. Techno-Economic and Environmental Assessment (Path C)

The economic and environmental analysis builds upon the performance of the MTHP, considering both operational energy balances and comparative savings relative to con-

ventional fossil-based systems. The measured heat output of the system was 705.5 MWh, delivered with a weighted average COP of 3.96. This corresponds to an electrical energy demand of 178.2 MWh/yr.

From an economic perspective, considering an initial investment cost of the MTHP equal to €80,000 and an annual net operating cash flow of €15,278 (already accounting for electricity expenditure, seasonal revenue losses, and maintenance costs), the MTHP installation provides a NPV of €127,633 over 20 years at a 4% discount rate [33]. The PBP is achieved in the sixth year of operation, as shown in Figure 12 along with Table 7 with a detailed cost breakdown. In addition, an LCOH of 0.0245 €/kWh was obtained, which is aligned with comparable studies on large-scale HP integration in DHNs that report LCOH values between 0.02 €/kWh and 0.04 €/kWh, depending on local electricity prices and load factors [34–37]. Furthermore, this value is markedly lower than conventional fossil-based options, which range from 0.1 €/kWh for natural gas boilers to 0.15 €/kWh for fuel-oil boilers, and up to 0.3 €/kWh for direct electric heating [38].

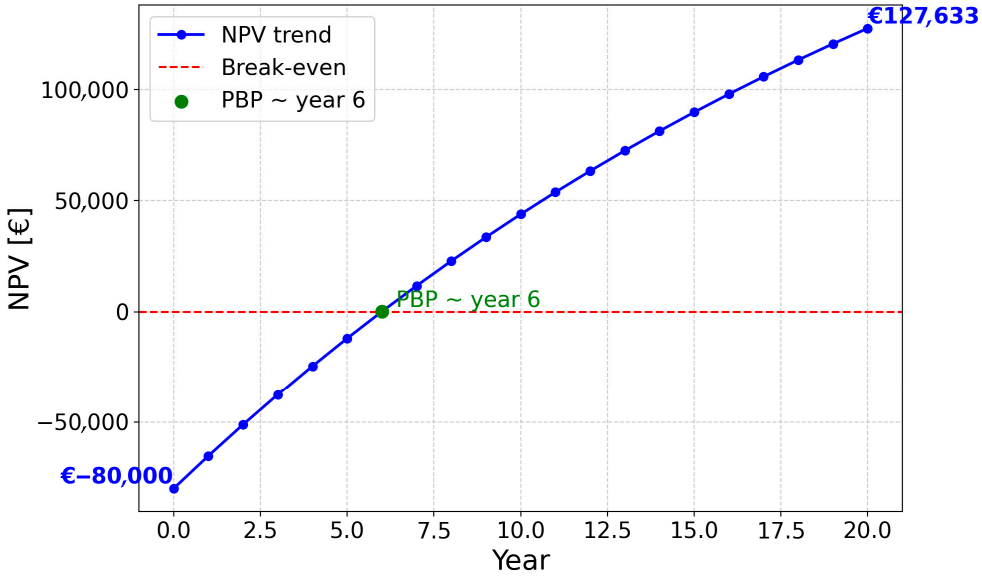

Figure 12. Cumulative discounted cash flow (NPV) over 20 years at 4% discount rate.

Table 7. Input data and cost/revenue assumptions for the MTHP case.

Item	Value [Unit of Measure]
Technology	MTHP
CAPEX	€80,000
Electricity cost (self-consumed)	0.055 €/kWh
Thermal energy tariff (revenue)	0.085 €/kWh
OPEX	0.30 €/OHs
Seasonal revenue losses—winter	26%
Seasonal revenue losses—non-winter	51%
Annual net operating cash flow	15,278 €/yr
Analysis horizon	20 years
Discount rate	4% [33]

From an environmental standpoint, the replacement of a conventional natural gas boiler with the multi-stage heat pump leads to substantial benefits in terms of Greenhouse Gas (GHG) emissions. Considering the Italian average emission factors of EF_{NG} = 0.209 $kgCO_2$/kWh [39] for natural gas combustion and EF_{el} = 0.246 $kgCO_2$/kWh [40] for electricity generation, the specific carbon intensity of the two systems differs markedly.

When accounting for the boiler efficiency (η_{boiler} = 0.9), the effective emission factor of the gas system amounts to 0.232 $kgCO_2/kWh$, while the HP, operating at a weighted average COP of 3.96, exhibits a much lower effective value of only 0.062 $kgCO_2/kWh$. On an annual basis, to deliver the required 705.5 MWh heat output, the gas boiler would release about 163.8 tCO_2, whereas the HP requires 178 MWh of electricity, resulting in 43.8 tCO_2 of indirect emissions. This corresponds to a net reduction of 120 tCO_2, which highlights the decisive contribution of HP electrification in decarbonising the heating sector, as shown in Figure 13.

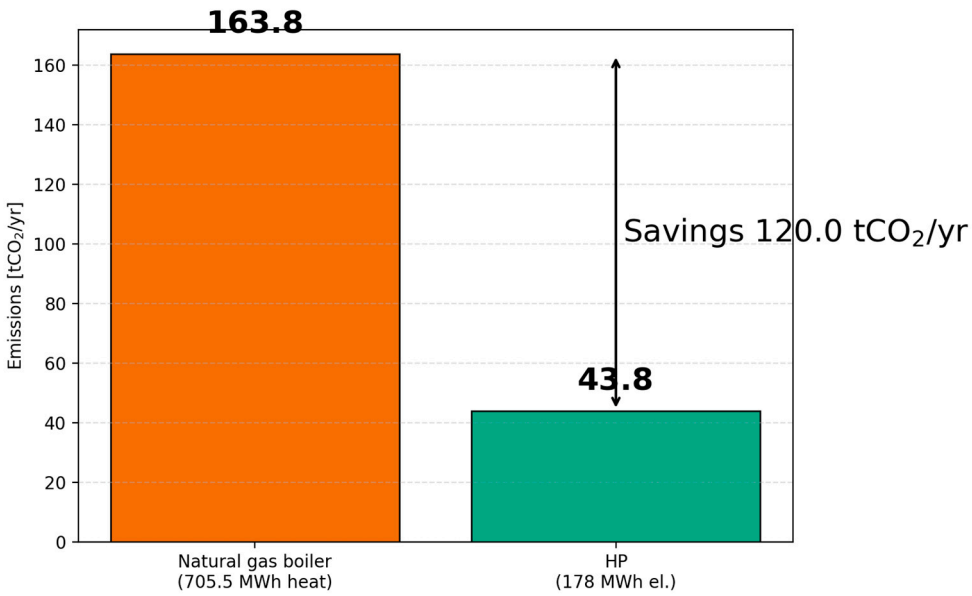

Figure 13. Comparison of CO_2 emissions from a natural gas boiler and the analysed MTHP.

These economic outcomes are particularly relevant for municipal utilities, as they demonstrate that MTHPs can reduce heating costs while improving environmental performance, thus supporting affordable and sustainable urban energy services.

From an urban sustainability perspective, the CO_2 savings highlight the contribution of MTHPs to local climate action plans and their potential role in enhancing air quality and resilience in cities.

6. Conclusions

This study presents a comprehensive assessment of a MTHP integrated into a small-scale DHN, demonstrating both the robustness of the design methodology and the effectiveness of the technology under real operating conditions.

The operating data showed that the MTHP operated almost continuously near its nominal design point, with a weighted average COP of 3.96 and a thermal output of 134.5 kW, closely aligned with the design values. The system maintained stable performance across the overall operational time, with 95% of the operating hours within a high-efficiency COP range of 3.5–4.5. The limited variability of the DHN return line played a key role in ensuring stable operation by minimising performance penalties associated with transient conditions. In addition, the surrogate modelling approach confirmed the robustness of the performance assessment, yielding interpretable correlations between efficiency, temperature lift, and mass flow rate.

From an economic standpoint, the installation proved financially attractive, yielding a positive NPV of €127,633 over a 20-year lifetime and achieving a payback period in the sixth year of operation. The LCOH was estimated at 0.0245 €/kWh, demonstrating strong competitiveness with conventional heating technologies. Compared with a

reference natural gas boiler, the system achieves annual CO_2 emission reductions of approximately 120 t, underscoring its environmental benefits and alignment with European decarbonisation objectives.

Beyond the technical validation of MTHPs in DHNs, this study has broader implications for energy and climate policy. The results demonstrate that MTHPs can enable cost-competitive decarbonisation of small- to medium-scale DHNs by exploiting stable low-grade return flow, a configuration that is widely replicable across European urban contexts. By achieving CO_2 emission reductions of approximately 120 t per year from a single installation, the technology directly supports EU climate objectives under the European Green Deal, REPowerEU, and the "Fit for 55" framework. From a strategic perspective, these findings provide practical evidence to support municipal utilities and policymakers in prioritising MTHP integration as a low-risk, near-term investment. Such systems offer an effective transition pathway between existing fossil-based district heating infrastructures and future renewable-driven heating systems, positioning MTHPs not only as a technical solution but also as a scalable policy lever for achieving long-term decarbonisation of the heating sector.

Overall, the results validate the design-phase assumptions and demonstrate that MTHPs can be effectively deployed in medium-temperature DHNs. Their capability to recover low-grade heat and upgrade it to network supply conditions positions MTHPs as a key enabler of efficient, electrified, and low-carbon heating systems. Future research should build on these findings by exploring hybrid system configurations and deeper integration with renewable energy sources to further enhance overall efficiency and long-term sustainability.

Author Contributions: Conceptualization, M.R., D.S., and G.C.; methodology, M.R. and D.S.; software, M.R.; validation, M.R. and D.S.; formal analysis, M.R. and G.C.; investigation, M.R. and D.S.; resources, D.S. and G.C.; data curation, M.R.; writing—original draft preparation, M.R., D.S., and G.C.; writing—review and editing, M.R., D.S., and G.C.; visualisation, M.R.; supervision, G.C. All authors have read and agreed to the published version of the manuscript.

Funding: This research received no external funding.

Data Availability Statement: The data supporting the findings of this study were provided by Astea S.p.A. under a confidentiality agreement and are not publicly available due to commercial sensitivity. Derived and processed data used in the analysis are available from the corresponding author on reasonable request for academic and non-commercial research purposes. No publicly archived datasets were generated during this study.

Acknowledgments: The authors would like to thank Astea S.p.A. for providing the operating and economic data of the MTHP. The authors would like to thank Eng. Angelo Di Rocco, and his Supervisor Giovanni Di Nicola, since he performed this work within his Master's thesis, providing a considerable and valuable help on the previous mentioned research project and on this analysis as well.

Conflicts of Interest: Author Danilo Salvi was employed by the company Astea S.p.A. The remaining authors declare that the research was conducted in the absence of any commercial or financial relationships that could be construed as a potential conflict of interest.

Abbreviations

The following abbreviations are used in this manuscript:

C	Compressor
CAPEX	CAPital EXpenditure
CHP	Combined Heat and Power
CO	Condenser

CO_2	Carbon dioxide
COP	Coefficient of Performance
COP_{Carnot}	Carnot Coefficient of Performance
DHN	District Heating Network
EU	European Union
EV	Evaporator
GHG	Greenhouse Gas
GWP	Global Warming Potential
HP	Heat Pump
HTHP	High-Temperature Heat Pump
LCOH	Levelised Cost of Heat
LHV	Lower Heating Value
LV	Lamination valve
MAE	Mean Absolute Error
MLR	Multiple Linear Regression
MTHP	Medium-Temperature Heat Pump
NOCS	Net Operating Cost Savings
NPV	Net Present Value
ODP	Ozone Depletion Potential
OHs	Operating Hours
OPEX	OPerational EXpenditure
PBP	PayBack Period
R^2	Determination coefficient
R&D	Research and Development
RE	Recuperator
RED	Renewable Energy Directive
RMSE	Root Mean Square Error
SQL	Structured Query Language
TRL	Technology Readiness Level

Nomenclature

c_{el} [€/kWh]	Electricity cost
CHP [€]	Heat pump cost rate
c_{NG} [€/kWh]	Natural gas cost
C_{NG} [€]	Boiler cost rate
CO_2^{HP} [$kgCO_2$]	Carbon Dioxide emission from heat pump
CO_2^{NG} [$kgCO_2$]	Carbon Dioxide emission from natural gas
c_p [kJ/kg × °C or kJ/kg × K]	Specific heat at constant pressure
c_{pin_EV} [kJ/kg × °C or kJ/kg × K]	Inlet specific heat at constant pressure in the EV
c_{pout_EV} [kJ/kg × °C or kJ/kg × K]	Outlet specific heat at constant pressure in the EV
ΔT_{EV} [°C or K]	Temperature difference across the EV
ΔT_{lift} [°C or K]	Temperature difference between DHN supply and return lines
ΔT_{CO} [°C or K]	Temperature difference across the CO
η_{II} [-]	Second-law efficiency
η_{boiler} [-]	Boiler thermal efficiency
EF_{el} [$kgCO_2$/kWh]	Emission factor from electric energy source
EF_{NG} [$kgCO_2$/kWh]	Emission factor from natural gas energy source
ΔCO_2 [$kgCO_2$]	Carbon Dioxide emission difference
ρ [kg/m^3]	Density
ρ_{in_EV} [kg/m^3]	Inlet density in the EV
ρ_{out_EV} [kg/m^3]	Outlet density in the EV
r	Discount rate
$\dot{m}_{EV}$ [kg/s]	Mass flow rate in the EV
$\dot{m}_{CO}$ [kg/s]	Mass flow rate in the CO
$\dot{m}_{R134a}$ [kg/s]	Mass flow rate of the Freon (1,1,1,2-tetrafluoroethane)

Q_{cond} [kW]	Thermal power output supplied to the DHN supply line
P_{el} [kW]	Electric power supplied to the modulating scroll compressor
Q_{evap} [kW]	Thermal power absorbed from the DHN return line
R134a	Freon (1,1,1,2-tetrafluoroethane)
T_{in_EV} [°C or K]	Inlet temperature in the EV
T_{out_EV} [°C or K]	Outlet temperature in the EV

References

1. European Commission. A European Green Deal: Striving to Be the First Climate-Neutral Continent. Available online: https://commission.europa.eu/strategy-and-policy/priorities-2019-2024/european-green-deal_en (accessed on 10 October 2025).
2. European Commission. REPowerEU: Affordable, Secure and Sustainable Energy for Europe. Available online: https://commission.europa.eu/topics/energy/repowereu_en (accessed on 10 October 2025).
3. European Commission. Renewable Energy Directive: Targets and Rules. Available online: https://energy.ec.europa.eu/topics/renewable-energy/renewable-energy-directive-targets-and-rules/renewable-energy-directive_en (accessed on 10 October 2025).
4. Council of the European Union. Fit for 55: Delivering the EU's 2030 Climate Target on the Way to Climate Neutrality. Available online: https://www.consilium.europa.eu/en/policies/fit-for-55/ (accessed on 10 October 2025).
5. Carvalho, J.P.; Lopes, E.B.; Santos, J.B.; Monteiro, J.; Cabrita, C.; Pacheco, A. Comparative Viability of Photovoltaic Investments Across European Countries Using Payback Periods and the Levelized Cost of Energy. *Energies* **2025**, *18*, 4676. [CrossRef]
6. Prajzendanc, P.; Kreischer, C. A Review of New Technologies in the Design and Application of Wind Turbine Generators. *Energies* **2025**, *18*, 4082. [CrossRef]
7. Kishore, T.S.; Patro, E.R.; Harish, V.S.K.V.; Haghighi, A.T. A Comprehensive Study on the Recent Progress and Trends in Development of Small Hydropower Projects. *Energies* **2021**, *14*, 2882. [CrossRef]
8. Zlateva, P.; Terziev, A.; Murzova, M.; Mileva, N.; Vassilev, M. Market Research on Waste Biomass Material for Combined Energy Production in Bulgaria: A Path Toward Enhanced Energy Efficiency. *Energies* **2025**, *18*, 4153. [CrossRef]
9. Ballerini, V.; Rossi di Schio, E.; Chekifi, T.; Valdiserri, P. Thermal Comfort and Energy Consumption in a Residential Building: An Experimental Comparison Between a Heat Pump and Gas Boiler Employing Low-Cost Microcontroller-Driven Sensors. *Energies* **2025**, *18*, 4398. [CrossRef]
10. Brodal, E. Heat Pump Optimization-Comparative Study of Different Optimization Algorithms and Heat Exchanger Area Approximations. *Energies* **2025**, *18*, 5270. [CrossRef]
11. Niknam, P.H. Low-Carbon Industrial Heating in the EU and UK: Integrating Waste Heat Recovery, High-Temperature Heat Pumps, and Hydrogen Technologies. *Energies* **2025**, *18*, 4313. [CrossRef]
12. IEA Heat Pumping Technologies Technical Collaboration Program. Annex 58: High Temperature Heat Pump Systems. Available online: https://heatpumpingtechnologies.org/annex58/ (accessed on 10 October 2025).
13. European Heat Pump Association (EHPA). Industrial Heat Pumps—Overview. December 2022. Available online: https://www.ehpa.org/wp-content/uploads/2022/12/Industrial-Heat-Pumps-overview.pdf (accessed on 10 October 2025).
14. National Renewable Energy Laboratory (NREL). *High-Temperature Heat Pump Model Documentation*; NREL Technical Report NREL/TP-7A40-84560; NREL: Golden, CO, USA, 2023. Available online: https://www.nrel.gov/docs/fy23osti/84560.pdf (accessed on 10 October 2025).
15. Yoo, J.; Estrada-Perez, C.E.; Choi, B.-H. Investigation of heat pump technologies for high-temperature applications above 250 °C. *Appl. Energy* **2025**, *384*, 125384. [CrossRef]
16. Ma, X.; Du, Y.; Zhao, T.; Zhu, T.; Lei, B.; Wu, Y. A comprehensive review of compression high-temperature heat pump steam system: Status and trend. *Int. J. Refrig.* **2024**, *164*, 218–242. [CrossRef]
17. Fernández-Moreno, A.; Mota-Babiloni, A.; Giménez-Prades, P.; Navarro-Esbrí, J. Optimal refrigerant mixture in single-stage high-temperature heat pumps based on a multiparameter evaluation. *Sustain. Energy Technol. Assess.* **2022**, *52*, 101989. [CrossRef]
18. Robbins, T.; Kini, G.; Garimella, S. Alternate control methods for adsorption heat pumps. *Int. J. Refrig.* **2020**, *120*, 127–136. [CrossRef]
19. Li, J.; Yang, Z.; Li, H.; Hu, S.; Duan, Y.; Yan, J. Optimal schemes and benefits of recovering waste heat from data center for district heating by CO_2 transcritical heat pumps. *Energy Convers. Manag.* **2021**, *245*, 114591. [CrossRef]
20. Yu, X.; Huang, G.; Hu, Z.; Yang, T.; Zou, H.; Tang, M. Performance assessment of high temperature heat pump working with different configurations in combination with internal heat exchanger, economizer and subcooler. *Energy* **2025**, *334*, 137727. [CrossRef]
21. Jodeiri, A.M.; Goldsworthy, M.J.; Buffa, S.; Cozzini, M. Role of sustainable heat sources in transition towards fourth generation district heating—A review. *Renew. Sustain. Energy Rev.* **2022**, *158*, 112156. [CrossRef]

22. Pakere, I.; Gravelsins, A.; Lauka, D.; Bazbauers, G.; Blumberga, D. Linking energy efficiency policies toward 4th generation district heating system. *Energy* **2021**, *234*, 121245. [CrossRef]
23. Reiners, T.; Gross, M.; Altieri, L.; Wagner, H.-J.; Bertsch, V. Heat pump efficiency in fifth generation ultra-low temperature district heating networks using a wastewater heat source. *Energy* **2021**, *236*, 121318. [CrossRef]
24. Lund, H.; Østergaard, P.A.; Nielsen, T.B.; Werner, S.; Thorsen, J.E.; Gudmundsson, O.; Arabkoohsar, A.; Mathiesen, B.V. Perspectives on fourth and fifth generation district heating. *Energy* **2021**, *277*, 120520. [CrossRef]
25. Mateu-Royo, C.; Sawalha, S.; Mota-Babiloni, A.; Navarro-Esbrí, J. High temperature heat pump integration into district heating network. *Energy Convers. Manag.* **2020**, *210*, 112719. [CrossRef]
26. Vivian, J.; Emmi, G.; Zarrella, A.; Jobard, X.; Pietruschka, D.; De Carli, M. Evaluating the cost of heat for end users in ultra low temperature district heating networks with booster heat pumps. *Energy* **2018**, *153*, 788–800. [CrossRef]
27. Barco-Burgos, J.; Bruno, J.C.; Eicker, U.; Saldaña-Robles, A.L.; Alcántar-Camarena, V. Review on the integration of high-temperature heat pumps in district heating and cooling networks. *Energy* **2022**, *239*, 122378. [CrossRef]
28. Corradi, E.; Rossi, M.; Mugnini, A.; Nadeem, A.; Comodi, G.; Arteconi, A.; Salvi, D. Energy, Environmental, and Economic Analyses of a District Heating (DH) Network from Both Thermal Plant and End-Users' Prospective: An Italian Case Study. *Energies* **2021**, *14*, 7783. [CrossRef]
29. Mugnini, A.; Comodi, G.; Arteconi, A. Heat pumps to upgrade existing CHP-DHN systems towards new generation thermal networks. *Energy Rep.* **2024**, *12*, 820–833. [CrossRef]
30. Zheng, X.; Chen, X.; Li, H.; Svendsen, S. Dynamic modelling and validation of low-temperature district heating systems considering fluctuating return temperatures. *Appl. Therm. Eng.* **2022**, *214*, 118749. [CrossRef]
31. Abbasi, M.H.; Abdullah, B.; Ahmad, M.W.; Rostami, A.; Cullen, J. Heat transition in the European building sector: Overview of the heat decarbonisation practices through heat pump technology. *Sustain. Energy Technol. Assess.* **2021**, *48*, 101630. [CrossRef]
32. Jiang, J.; Yu, H.; Song, G.; Zhao, J.; Zhao, K.; Ji, H.; Li, P. Surrogate model assisted multi-criteria operation evaluation of community integrated energy systems. *Sustain. Energy Technol. Assess.* **2022**, *53*, 102656. [CrossRef]
33. Kapıcıoğlu, A.; Esen, H. Economic and environmental assessment of ground source heat pump system: The case of Turkey. *Sustain. Energy Technol. Assess.* **2022**, *53*, 102562. [CrossRef]
34. Rizi, B.S.; Lee, J.; Heidarinejad, M. Trends for the installation of heat pumps in the US residential buildings. *Sustain. Energy Technol. Assess.* **2025**, *73*, 104080. [CrossRef]
35. Aditya, G.R.; Mikhaylova, O.; Narsilio, G.A.; Johnston, I.W. Comparative costs of ground source heat pump systems against other forms of heating and cooling for different climatic conditions. *Sustain. Energy Technol. Assess.* **2020**, *42*, 100824. [CrossRef]
36. Calise, F.; Cappiello, F.L.; Dentice d'Accadia, M.; Petrakopoulou, F.; Vicidomini, M. A solar-driven 5th generation district heating and cooling network with ground-source heat pumps: A thermo-economic analysis. *Sustain. Cities Soc.* **2022**, *76*, 103438. [CrossRef]
37. Sadeghi, H.; Ijaz, A.; Singh, R.M. Current status of heat pumps in Norway and analysis of their performance and payback time. *Sustain. Energy Technol. Assess.* **2022**, *54*, 102829. [CrossRef]
38. Maruf, M.N.I.; Morales-España, G.; Sijm, J.; Helistö, N.; Kiviluoma, J. Classification, potential role, and modeling of power-to-heat and thermal energy storage in energy systems: A review. *Sustain. Energy Technol. Assess.* **2022**, *53*, 102553. [CrossRef]
39. ISPRA (Istituto Superiore per la Protezione e la Ricerca Ambientale), Inventario Nazionale-Emissioni in Atmosfera, Web Portal, Annually Updated-Includes the National Inventory Report (NIR) and Informative Inventory Report (IIR), Containing Greenhouse Gas and Pollutant Emissions Data Consistent with UNFCCC Formats, Methodology Descriptions, and QA/QC Procedures. Available online: https://emissioni.sina.isprambiente.it/inventario-nazionale/ (accessed on 10 October 2025).
40. Caputo, A. *Rapporti 343/2021—Monitoraggio e Prevenzione Degli Impatti Sull'atmosfera, Istituto Superiore per la Protezione e la Ricerca Ambientale (ISPRA); Rapporto No. 343/2021*; Politecnico di Milano: Milan, Italy, 2021; ISBN 978-88-448-1049-8. Available online: https://www.politesi.polimi.it/retrieve/aaade1a2-2ef3-42b3-a53d-dffbe0bb5e99/2022_12_Capparelli.pdf (accessed on 10 October 2025).